Acta Mech 231, 2895–2913 (2020)
https://doi.org/10.1007/s00707-020-02679-7

ORIGINAL PAPER

D. K. Yi · T. C. Wang

On the effect of an out-of-plane constraint on the three-dimensional crack front fields in a thin elastic plate

Received: 11 November 2019 / Revised: 21 March 2020 / Published online: 29 April 2020

Abstract Two-dimensional theories of fracture are still applied widely today and provide theoretical foundations for solutions to many practical problems. These two-dimensional theories are based on the plane strain or plane stress assumption. However, strictly speaking, for a thin elastic plate with a through-thickness crack under tension, plane strain conditions can be met only at the crack front (except the corn point) and plane stress conditions exist at a distance of about one half of the plate thickness from the crack front in the mid-plane. What are the stress fields in the region where both plane strain and plane stress conditions cannot be met? In this paper, further investigations into the problem are carried out. Three-dimensional Maxwell stress functions, the principle of minimum complementary potential energy and three-dimensional J-integrals are employed to obtain an analytical solution to depict the relationship among out-of-plane constraints, three-dimensional J-integrals and stress intensity factors. Three-dimensional finite element simulations with fine meshes are carried out to verify the analytical results. Compared with the corresponding plane strain solution, the solution proposed is valid in a larger region.

1 Introduction

Solutions based on two-dimensional theories of fracture are accurate enough for many practical problems. However, there are some examples that these two-dimensional theories result in a distorted view of reality [1]. Undoubtedly, three-dimensional fracture analysis is needed to fully understand fracture behavior of materials, and the study of three-dimensional fracture has been an important issue in fracture mechanics.

In earlier studies, Hartranft and Sih [2] and Sih [3] derived an asymptotic solution for the three-dimensional stress fields near the front of a crack in an elastic plate under tension. Considering a quarter of infinite crack plane in a half space, Benthem [4] investigated the singularity at a corner point (intersection of the crack front and the free surface). Benthem concluded that the singularity at a corner point is weaker than the square-root singularity. Using a separable eigen-function approach, Kawai et al. [5] derived a solution for the stress fields near a corner point, which are expressed as the superimposition of three kinds of singular terms. Yang and Freud [6] studied the state of stress in a thin elastic plate containing a through-thickness crack under Mode-I loading and derived a solution in the form of a real integral for the stress fields near the crack front. They showed that a finite lateral contraction appears at the crack front, and the proposed solution merges smoothly with the corresponding plane stress solution at a distance of one half of the plate thickness from the crack front. Nakamura and Parks [7] carried out a stress analysis for a thin cracked elastic plate under

D. K. Yi (✉)
College of Mechanics and Materials, Hohai University, Nanjing, China
E-mail: csruydk@163.com

T. C. Wang
LNM, Institute of Mechanics, Chinese Academy of Science, Beijing, China

tension using three-dimensional finite element methods. They revealed that three-dimensional effects vanish at a radial distance of one half of the plate thickness from the crack front in the mid-plane. These authors argued that their numerical results for the stress fields near the corner point are consistent with Benthem's solutions [4]. Pook [8–10] presented some theoretical solutions for corner point singularities. He believed that corner point singularities exist, but there are only limited cases that these singularities should be considered. Using a method of separation of variables, Leung and Su [11] presented an analytical solution for Mode-I cracking in a semi-infinite domain. The solution gave an explanation for the phenomena that stress intensity factors decrease sharply in the region very close to the surface (also called boundary layer). Considering an elastic plate with a through-thickness crack, Kwon and Sun [12] presented three-dimensional finite element results of the crack front stress fields in the boundary layer. These authors argued that the solution for the crack front stress fields in the boundary layer can be expressed as the superimposition of the corner singularity field solution and the classic K-field solution. Noda [13] proposed stress intensity evaluation formulae for a three-dimensional crack under mixed mode loading and also the crack terminating at an interface between bi-materials. In his paper, the author argued that the maximum stress intensity factor $K_{\max}$ is proportional to $\sqrt{A_r}^{1-\eta}$. Here, A_r is the area of the crack and η is the eigen-root determined by Dundurs' parameters. Using three-dimensional dislocation technologies, Kotousov [14] investigated the effect of plate thickness on the stress fields near the front of a through-thickness crack in an elastic plate under in-plane loading. Kotousov concluded that there is a new mode of singularity (the out-of-plane mode) in angular sectors subjected to in-plane loading. Using a complex variable method, Luo and Wang [15] presented a solution for the elastic fields in an infinite matrix containing an elliptic nano-inhomogeneity under anti-plane shear. Hutar et al. [16] investigated the effect of corner singularities on fatigue crack behavior. They concluded that corner singularities decrease fatigue crack propagation rates and result in a curved shape of crack front. Kotousov et al. [17] compared the difference between three-dimensional crack front stress fields and the corresponding two-dimensional crack tip stress fields for a cracked elastic plate under remote loading. These authors argued that 5 singularity modes appear in a real three-dimensional problem, while there are only 3 singularity modes in the classical theories of fracture. Considering multiple cracks and inhomogeneous inclusions beneath a half-space surface under contact loading, Zhou and Wei [18,19] proposed a semi-analytic formula to describe the relationship among surface deformation, pressure, and subsurface stress fields. He and Kotousov [20] carried out an experimental study to evaluate the effect of corner singularities. Their experimental results showed that the crack front fields in the region close to the surface of a cracked plate are significantly affected by the corner singularity. Considering a very small corner crack at a silicon-resin interface under tensile loading, Koguchi and Yokoyama [21] proposed a solution to depict the variation of mode-II stress intensity factors along the crack front using boundary element methods. Soliman et al. [22] proposed a new expression of three-dimensional J-integrals for studying the fracture process in elements. Considering a cracked infinite elastic plate under in-plane and out-of-plane loads, Chaudhuri [23] presented a rigorous approach to investigate the through-thickness variation of stress intensity factors and energy release rates. The solutions proposed can explain the phenomenon that Mode-I stress intensity factors decrease rapidly when approaching the free surface. Ludwig et al. [24] presented a new three-dimensional criterion for anisotropic crack growth in nickel based alloys under thermo-mechanical fatigue.

In most papers motioned above, the coefficient K (or the stress intensify factor) is considered as a function of the thickness-wise coordinate or thickness of a plate. These solutions may be accurate enough when plane strain conditions are met. However, what are the stress fields in the region where plane strain conditions gradually change into plane stress conditions? In our previous paper [25], the effect of an out-of-plane constraint on the crack front fields in the thickness direction is examined. In this paper, further investigations on the problem are carried out. The variations of out-of-plane constraints in the thickness and radial directions are investigated, and the effects of out-of-plane constraints on the crack front stress fields are depicted by analytical solutions. A series of new analytic results have been presented and compared with the corresponding numerical results. Fitting equations for out-of-plane constraints and three-dimensional J-integrals have been obtained for possible engineering applications.

2 Basic equations

The stress–strain relation of certain elastic materials in a cylindrical coordinate system shown in Fig. 1 may be written as

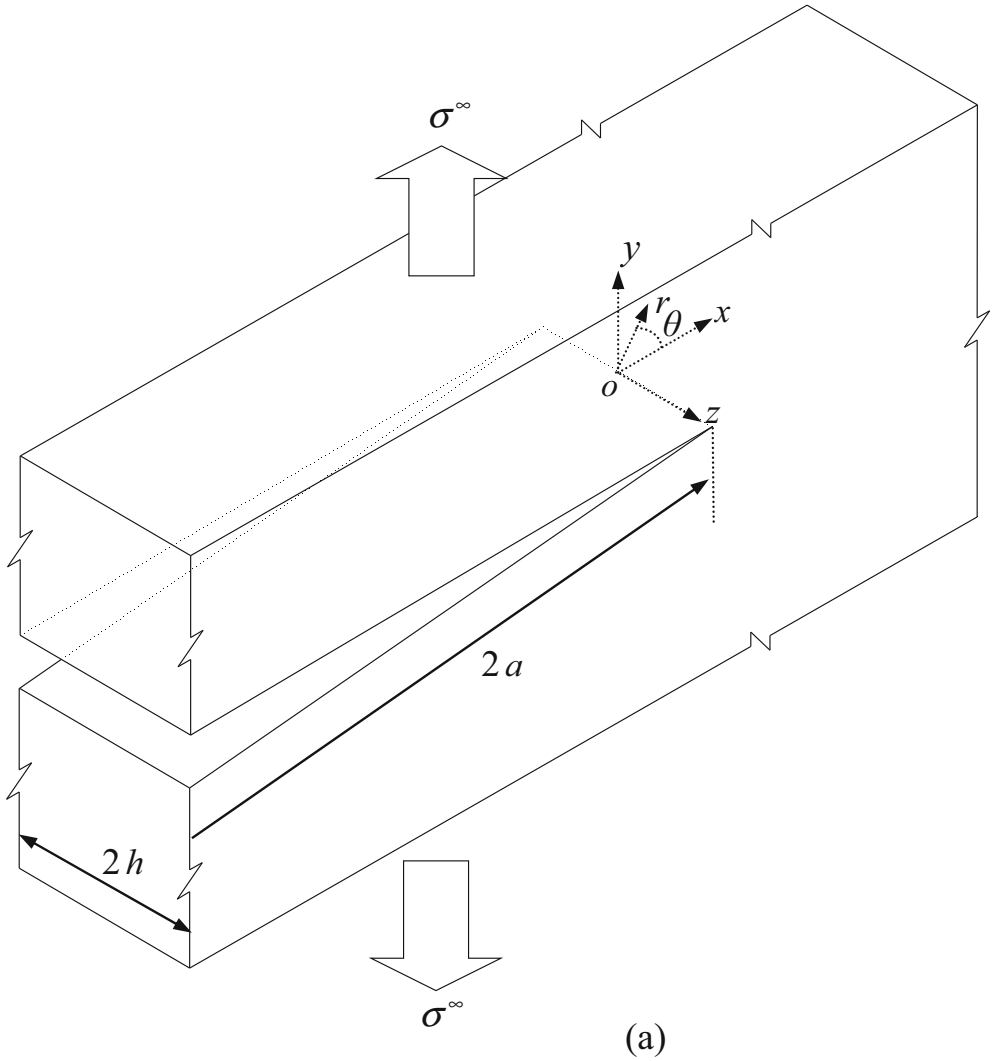

Fig. 1 A thin plate containing a through-thickness crack subjected to remote uniform tensile loading σ^{∞}

$$\varepsilon_r = \frac{\sigma_r - v\,(\sigma_\theta + \sigma_z)}{E}, \quad \varepsilon_\theta = \frac{\sigma_\theta - v\,(\sigma_r + \sigma_z)}{E}, \quad \varepsilon_{r\theta} = \frac{(1+v)}{E}\sigma_{r\theta},$$
$$\varepsilon_z = \frac{\sigma_z - v\,(\sigma_r + \sigma_\theta)}{E}, \quad \varepsilon_{rz} = \frac{(1+v)}{E}\sigma_{rz}, \quad \varepsilon_{\theta z} = \frac{(1+v)}{E}\sigma_{\theta z}. \tag{1}$$

Here, E represents Young's modulus and v represents Poisson's ratio.

When Maxwell stress functions (ϕ_i, $i = 1, 2, 3$) are introduced, stress components in the cylindrical coordinate system may be expressed as

$$\sigma_r = \cos^2\theta\frac{\partial^2\phi_2}{\partial z^2} + \sin^2\theta\frac{\partial^2\phi_1}{\partial z^2} + \frac{1}{r}(\phi_3)' + \frac{1}{r^2}(\phi_3)^{\cdot\cdot},$$
$$\sigma_\theta = \sin^2\theta\frac{\partial^2\phi_2}{\partial z^2} + \cos^2\theta\frac{\partial^2\phi_1}{\partial z^2} + (\phi_3)'',$$
$$\sigma_{r\theta} = -\frac{\sin 2\theta}{2}\left(\frac{\partial^2\phi_2}{\partial z^2} - \frac{\partial^2\phi_1}{\partial z^2}\right) + \frac{1}{r^2}(\phi_3)^{\cdot} - \frac{1}{r}(\phi_3)^{\cdot\prime},$$
$$\sigma_z = \sin^2\theta\,(\phi_1)'' + \frac{2\sin\theta\cos\theta}{r}(\phi_1)^{\cdot\prime} + \frac{\cos^2\theta}{r}(\phi_1)' - \frac{2\sin\theta\cos\theta}{r^2}(\phi_1)^{\cdot} + \frac{\cos^2\theta}{r^2}(\phi_1)^{\cdot\cdot}$$

$$+\cos^2\theta\,(\phi_2)^{''}-\frac{2\sin\theta\cos\theta}{r}(\phi_2)^{\cdot\prime}+\frac{\sin^2\theta}{r}(\phi_2)^{\prime}+\frac{2\sin\theta\cos\theta}{r^2}(\phi_2)^{\cdot}+\frac{\sin^2\theta}{r^2}(\phi_2)^{\cdot\cdot},$$

$$\sigma_{rz}=-\sin\theta\left(\sin\theta\frac{\partial(\phi_1)^{\prime}}{\partial z}+\frac{\cos\theta}{r}\frac{\partial(\phi_1)^{\cdot}}{\partial z}\right)-\cos\theta\left(\cos\theta\frac{\partial(\phi_2)^{\prime}}{\partial z}-\frac{\sin\theta}{r}\frac{\partial(\phi_2)^{\cdot}}{\partial z}\right),$$

$$\sigma_{\theta z}=-\cos\theta\left(\sin\theta\frac{\partial(\phi_1)^{\prime}}{\partial z}+\frac{\cos\theta}{r}\frac{\partial(\phi_1)^{\cdot}}{\partial z}\right)+\sin\theta\left(\cos\theta\frac{\partial(\phi_2)^{\prime}}{\partial z}-\frac{\sin\theta}{r}\frac{\partial(\phi_2)^{\cdot}}{\partial z}\right). \tag{2}$$

Here, $()^{\cdot}=\frac{\partial}{\partial\theta}$ and $()^{\prime}=\frac{\partial}{\partial r}$.

It can be proved that Eq. (2) satisfies the following equilibrium equations:

$$\begin{aligned}
&(\sigma_r)^{\prime}+\frac{1}{r}(\sigma_{r\theta})^{\cdot}+\frac{\partial\sigma_{rz}}{\partial z}+\frac{\sigma_r-\sigma_\theta}{r}=0,\\
&(\sigma_{r\theta})^{\prime}+\frac{1}{r}(\sigma_\theta)^{\cdot}+\frac{\partial\sigma_{\theta z}}{\partial z}+\frac{2\sigma_{r\theta}}{r}=0,\\
&(\sigma_{rz})^{\prime}+\frac{1}{r}(\sigma_{\theta z})^{\cdot}+\frac{\partial\sigma_z}{\partial z}+\frac{\sigma_{rz}}{r}=0.
\end{aligned} \tag{3}$$

3 Three-dimensional crack front fields

3.1 Expressions of stress–strain fields near the crack front

We consider a cracked thin plate under remote tension, shown in Fig. 1. Stress functions are attempted to be expressed as

$$\begin{aligned}
&\phi_1=\phi_2=F_1(z,r)\,r^{\frac{3}{2}}\tilde{\phi}_1(\theta),\\
&\phi_3=\phi=F(z,r)\,r^{\frac{3}{2}}\tilde{\phi}(\theta).
\end{aligned} \tag{4}$$

Here, we assume that

$$\lim_{r\to0}\left(\frac{\partial^{(n)}F_1(z,r)}{\partial r^n},\frac{\partial^{(n)}F_1(z,r)}{\partial z^n},\frac{\partial^{(n)}F(z,r)}{\partial r^n},\frac{\partial^{(n)}F(z,r)}{\partial z^n}\right)\neq\infty,\quad n=0,1,2,3,4; \tag{5}$$

when r tends to 0, one may find

$$\lim_{r\to0}\left(\frac{\partial^2\phi_1}{\partial z^2},\frac{\partial^2\phi_1}{\partial r\partial z},\frac{\partial^2\phi_1}{r\partial\theta\partial z}\right)=0. \tag{6}$$

Substituting Eq. (4) into the expressions of stress components [Eq. (2)] and noting Eqs. (5) and (6), the stress components near the crack front may be re-written as

$$\begin{aligned}
\sigma_r&\cong\frac{1}{r}(\phi)^{\prime}+\frac{1}{r^2}(\phi)^{\cdot\cdot}=F(z,r)\left(\frac{3}{2}\tilde{\phi}+\left(\tilde{\phi}\right)^{\cdot\cdot}\right)r^{-\frac{1}{2}},\\
\sigma_\theta&\cong(\phi)^{''}=\frac{3}{4}F(z,r)\,\tilde{\phi}r^{-\frac{1}{2}},\\
\sigma_{r\theta}&\cong\frac{1}{r^2}(\phi)^{\cdot}-\frac{1}{r}(\phi)^{\cdot\prime}=-\frac{1}{2}F(z,r)\left(\tilde{\phi}\right)^{\cdot}r^{-\frac{1}{2}},\\
\sigma_z&=(\phi_1)^{''}+\frac{1}{r}(\phi_1)^{\prime}+\frac{1}{r^2}(\phi_1)^{\cdot\cdot}=F_1(z,r)\left(\frac{9}{4}\tilde{\phi}_1+\left(\tilde{\phi}_1\right)^{\cdot\cdot}\right)r^{-\frac{1}{2}},\\
\sigma_{rz}&\cong0,\\
\sigma_{\theta z}&\cong0.
\end{aligned} \tag{7}$$

Substituting Eq. (7) into Eq. (1), the strain components near the crack front may be written as

$$\begin{aligned}
\varepsilon_r &= \frac{-v\left(\phi+\phi_1\right)^{''}+\frac{1-v}{r}\left(\phi\right)^{'}+\frac{1-v}{r^2}\left(\phi\right)^{\cdot\cdot}}{E},\\
\varepsilon_\theta &= \frac{\left(\phi\right)^{''}-v\left(\left(\phi_1\right)^{''}+\frac{1}{r}\left(\phi+\phi_1\right)^{'}+\frac{1}{r^2}\left(\phi+\phi_1\right)^{\cdot\cdot}\right)}{E},\\
\varepsilon_{r\theta} &= \frac{(1+v)}{E}\left(\frac{1}{r^2}\left(\phi\right)^{\cdot}-\frac{1}{r}\left(\phi\right)^{\cdot'}\right),\\
\varepsilon_z &= \frac{\left(\phi_1-v\phi\right)^{''}+\frac{1}{r}\left(\phi_1-v\phi\right)^{'}+\frac{1}{r^2}\left(\phi_1-v\phi\right)^{\cdot\cdot}}{E},\\
\varepsilon_{rz} &= 0,\\
\varepsilon_{\theta z} &= 0.
\end{aligned} \tag{8}$$

According to the principle of minimum complementary potential energy and employing the variational method, one may obtain partial differential governing equations, written as

$$\begin{aligned}
&\left(r\varepsilon_\theta\right)^{''}+\frac{\left(\varepsilon_r\right)^{\cdot\cdot}}{r}-\left(\varepsilon_r\right)^{'}-2\left(\varepsilon_{r\theta}\right)^{\cdot'}-2\left(\frac{\varepsilon_{r\theta}}{r}\right)^{\cdot}=0,\\
&\left(r\varepsilon_z\right)^{''}+\left(\frac{\varepsilon_z}{r}\right)^{\cdot\cdot}-\left(\varepsilon_z\right)^{'}=0.
\end{aligned} \tag{9}$$

The derivation of Eq. (9) is presented in the Appendix.

Substituting Eq. (8) into Eq. (9), one may obtain

$$\begin{aligned}
&\nabla^4\left(\phi-v\phi_1\right)=0,\\
&\nabla^4\left(\phi_1-v\phi\right)=0.
\end{aligned} \tag{10}$$

Then, one has

$$\begin{aligned}
&\nabla^4\left(\phi\right)=0,\ \nabla^4\left(\phi_1\right)=0,\\
&\nabla^4=\left(\frac{\partial^2}{\partial r^2}+\frac{\partial}{r\partial r}+\frac{\partial^2}{r^2\partial\theta^2}\right)\left(\frac{\partial^2}{\partial r^2}+\frac{\partial}{r\partial r}+\frac{\partial^2}{r^2\partial\theta^2}\right).
\end{aligned} \tag{11}$$

Substituting Eq. (4) into Eq. (11), one may have

$$\begin{aligned}
&F\left(z,r\right)\left(\tilde{\phi}\right)^{\cdot\cdot\cdot\cdot}+\left(\frac{5}{2}F\left(z,r\right)+4\left(F\left(z,r\right)\right)^{'}r+2\left(F\left(z,r\right)\right)^{''}r^2\right)\left(\tilde{\phi}\right)^{\cdot\cdot}\\
&+\left(\frac{9}{16}F\left(z,r\right)+\left(F\left(z,r\right)\right)^{'}r+\frac{25}{2}\left(F\left(z,r\right)\right)^{''}r^2+8\left(F\left(z,r\right)\right)^{'''}r^3+\left(F\left(z,r\right)\right)^{''''}r^4\right)\tilde{\phi}=0,\\
&F_1\left(z,r\right)\left(\tilde{\phi}_1\right)^{\cdot\cdot\cdot\cdot}+\left(\frac{5}{2}F_1\left(z,r\right)+4\left(F_1\left(z,r\right)\right)^{'}r+2\left(F_1\left(z,r\right)\right)^{''}r^2\right)\left(\tilde{\phi}_1\right)^{\cdot\cdot}\\
&+\left(\frac{9}{16}F_1\left(z,r\right)+\left(F_1\left(z,r\right)\right)^{'}r+\frac{25}{2}\left(F_1\left(z,r\right)\right)^{''}r^2+8\left(F_1\left(z,r\right)\right)^{'''}r^3+\left(F_1\left(z,r\right)\right)^{''''}r^4\right)\tilde{\phi}_1=0.
\end{aligned} \tag{12}$$

Noting Eq. (5) and ignoring the terms containing r, r^2, r^3, and r^4, Eq. (12) may be re-written as

$$\begin{aligned}
&\left(\tilde{\phi}\right)^{\cdot\cdot\cdot\cdot}+\frac{5}{2}\left(\tilde{\phi}\right)^{\cdot\cdot}+\frac{9}{16}\tilde{\phi}=0,\\
&\left(\tilde{\phi}_1\right)^{\cdot\cdot\cdot\cdot}+\frac{5}{2}\left(\tilde{\phi}_1\right)^{\cdot\cdot}+\frac{9}{16}\tilde{\phi}_1=0.
\end{aligned} \tag{13}$$

The general solutions for Eq. (13) may be expressed as

$$\tilde{\phi}\left(\theta\right)=A\cos\frac{\theta}{2}+B\sin\frac{\theta}{2}+C\cos\frac{3}{2}\theta+D\sin\frac{3}{2}\theta,$$

$$\tilde{\phi}_1(\theta) = A_1 \cos\frac{\theta}{2} + B_1 \sin\frac{\theta}{2} + C_1 \cos\frac{3}{2}\theta + D_1 \sin\frac{3}{2}\theta. \tag{14}$$

Boundary and symmetry conditions require

$$\begin{aligned} &\sigma_\theta(r, \pm\pi, z) = 0, \quad \sigma_{r\theta}(r, 0, z) = 0, \quad \sigma_{r\theta}(r, \pm\pi, z) = 0, \\ &\sigma_z(r, \theta, z) = \sigma_z(r, -\theta, z). \end{aligned} \tag{15}$$

Then, Eq. (14) may be re-written as

$$\begin{aligned} \tilde{\phi} &= A\left(\cos\frac{1}{2}\theta + \frac{1}{3}\cos\frac{3}{2}\theta\right), \\ \tilde{\phi}_1 &= A_1 \cos\frac{1}{2}\theta + C_1 \cos\frac{3}{2}\theta + D_1 \sin\frac{3}{2}\theta. \end{aligned} \tag{16}$$

Substituting Eq. (16) into the stress components in Eq. (7) and letting

$$\begin{aligned} \frac{K(z,r)}{\sqrt{2\pi}} &= F(z,r)\,A, \\ \frac{K_1(z,r)}{\sqrt{2\pi}} &= F_1(z,r)\,A_1, \end{aligned} \tag{17}$$

one may have

$$\begin{aligned} \sigma_r &= \frac{K(z,r)}{4\sqrt{2\pi r}}\left(5\cos\frac{\theta}{2} - \cos\frac{3}{2}\theta\right), \\ \sigma_\theta &= \frac{K(z,r)}{4\sqrt{2\pi r}}\left(3\cos\frac{\theta}{2} + \cos\frac{3}{2}\theta\right), \\ \sigma_{r\theta} &= \frac{K(z,r)}{4\sqrt{2\pi r}}\left(\sin\frac{\theta}{2} + \sin\frac{3}{2}\theta\right), \\ \sigma_z &= \frac{2K_1(z,r)}{\sqrt{2\pi r}}\cos\frac{\theta}{2}, \\ \sigma_{rz} &\cong 0, \\ \sigma_{\theta z} &\cong 0 \end{aligned} \tag{18}$$

or

$$\begin{aligned} \sigma_x &= \frac{\sigma_r + \sigma_\theta}{2} + \frac{\sigma_r - \sigma_\theta}{2}\cos 2\theta - \sigma_{r\theta}\sin 2\theta = \frac{K(z,r)}{\sqrt{2\pi r}}\cos\frac{\theta}{2}\left(1 - \sin\frac{1}{2}\theta\sin\frac{3}{2}\theta\right), \\ \sigma_y &= \frac{\sigma_r + \sigma_\theta}{2} - \frac{\sigma_r - \sigma_\theta}{2}\cos 2\theta + \sigma_{r\theta}\sin 2\theta = \frac{K(z,r)}{\sqrt{2\pi r}}\cos\frac{\theta}{2}\left(1 + \sin\frac{1}{2}\theta\sin\frac{3}{2}\theta\right), \\ \tau_{xy} &= \frac{\sigma_r - \sigma_\theta}{2}\sin 2\theta + \sigma_{r\theta}\cos 2\theta = \frac{K(z,r)}{\sqrt{2\pi r}}\cos\frac{\theta}{2}\sin\frac{\theta}{2}\cos\frac{3}{2}\theta, \\ \sigma_z &= \frac{2K_1(z,r)}{\sqrt{2\pi r}}\cos\frac{\theta}{2} = \frac{2T_z(z,r)\,K(z,r)}{\sqrt{2\pi r}}\cos\frac{\theta}{2}, \\ \sigma_{rz} &\cong 0, \\ \sigma_{\theta z} &\cong 0. \end{aligned} \tag{19}$$

Here, $T_z(z,r)$ is the out-of-plane constraint defined as

$$T_z(z,r) = \frac{\sigma_z}{\sigma_x + \sigma_y} = \frac{K_1(z,r)}{K(z,r)}, \quad 0 \le T_z(z,r) \le v. \tag{20}$$

Substituting Eq. (18) into Eq. (1), the expressions of strain components may be re-written as

$$\varepsilon_r = \frac{K(z,r)}{4E\sqrt{2\pi r}}\left((5 - 3v - 8vT_z(z,r))\cos\frac{1}{2}\theta - (1+v)\cos\frac{3}{2}\theta\right),$$

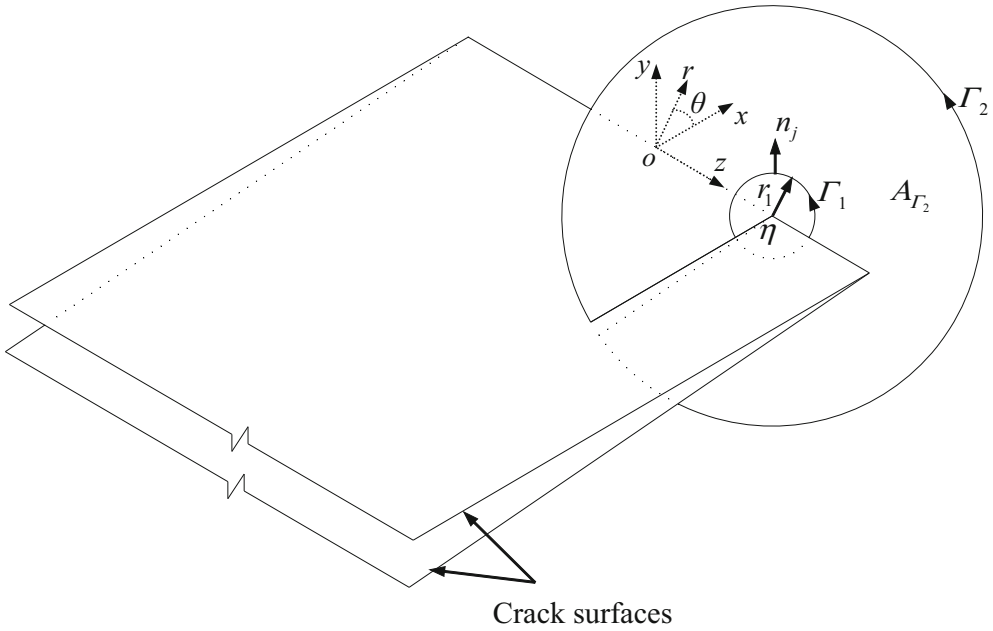

Fig. 2 J-integral for three-dimensional fracture

$$\begin{aligned}
\varepsilon_\theta &= \frac{K(z,r)}{4E\sqrt{2\pi r}}\left((3-5v-8vT_z(z,r))\cos\frac{1}{2}\theta+(1+v)\cos\frac{3}{2}\theta\right),\\
\varepsilon_{r\theta} &= \frac{K(z,r)}{4E\sqrt{2\pi r}}(1+v)\left(\sin\frac{1}{2}\theta+\sin\frac{3}{2}\theta\right),\\
\varepsilon_z &= \frac{2K(z,r)}{E\sqrt{2\pi r}}(T_z(z,r)-v)\cos\frac{1}{2}\theta,\\
\gamma_{zr} &= 0,\\
\gamma_{z\theta} &= 0.
\end{aligned} \tag{21}$$

When r is zero, T_z should equal v in order to meet plane strain conditions.

3.2 Expression of $K(r, z)$

A three-dimensional J-integral [26–29] may be written as

$$\begin{aligned}
J(\eta) &= \lim_{r_1\to 0}\int_{\Gamma_1}\left(W\mathrm{d}y-\sigma_{ij}n_j u_{i,x}\mathrm{d}s\right),\\
&= \int_{\Gamma_2}\left(W\mathrm{d}y-\sigma_{ij}n_j u_{i,x}\mathrm{d}s\right)-\int_{A(\Gamma_2)}\frac{\partial\left(\sigma_{iz}u_{i,x}\right)}{\partial z}\mathrm{d}A(\Gamma_2), \quad i=x,y,z,\ j=x,y.
\end{aligned} \tag{22}$$

Here, $J(\eta)$ represents the J-integral at a given point η along the crack front shown in Fig. 2. W is the strain energy density, σ_{ij} and u_i are stress and displacement components separately. Both path Γ_1 and path Γ_2 lie in the plane perpendicular to the crack front, and n_j are the components of a unit vector outward normal to the integral paths and normal to the crack front. A_{Γ_2} represents the region bounded by Γ_2.

The integral of the strain energy density W along the path Γ_1 may be expressed as

$$\int_{\Gamma_1} W\mathrm{d}y=\int_{-\pi}^{\pi}Wr_1\cos\theta\mathrm{d}\theta\cong\int_{-\pi}^{\pi}\frac{1}{2}\left(\sigma_r\varepsilon_r+\sigma_\theta\varepsilon_\theta+\sigma_z\varepsilon_z+2\sigma_{r\theta}\varepsilon_{r\theta}\right)r_1\cos\theta\mathrm{d}\theta. \tag{23}$$

Substituting Eqs. (18) and (21) into Eq. (23), one may obtain

$$\begin{aligned}\int_{\Gamma_1} W\mathrm{d}y &= \frac{K^2(z,r)}{64\pi E}\int_{-\pi}^{\pi}\left\{\left(34-30v-128vT_z(z,r)+64\left(T_z(z,r)\right)^2\right)\left(\cos\frac{\theta}{2}\right)^2\right.\\ &\left.+2(1+v)\left(\cos\frac{3}{2}\theta\right)^2-4(1+v)\cos\frac{3}{2}\theta\cos\frac{\theta}{2}+2(1+v)\left(\sin\frac{\theta}{2}+\sin\frac{3}{2}\theta\right)^2\right\}\cos\theta\mathrm{d}\theta\\ &= \frac{K^2(z,r)}{4E}\left(2\left(T_z(z,r)\right)^2-4vT_z(z,r)-v+1\right).\end{aligned} \tag{24}$$

Similarly, the second integral in the first line in Eq. (22) may be expressed as [30]

$$\begin{aligned}-\int_{\Gamma_1}\sigma_{ij}n_ju_{i,x}\mathrm{d}s &= -\int_{-\pi}^{\pi}\left(\sigma_xn_xu_{x,x}+\sigma_{xy}n_yu_{x,x}+\sigma_{xy}n_xu_{y,x}+\sigma_yn_yu_{y,x}\right)r_1\mathrm{d}\theta\\ &= -\int_{-\pi}^{\pi}\left[\sigma_r\left(-\frac{\sin\theta}{r_1}\left((u_r)^{\cdot}-(u_\theta)\right)+(u_r)'\cos\theta\right)\right.\\ &\left.+\sigma_{r\theta}\left(-\frac{\sin\theta}{r_1}\left((u_\theta)^{\cdot}+u_r\right)+\cos\theta\,(u_\theta)'\right)\right]r_1\mathrm{d}\theta.\end{aligned} \tag{25}$$

Using the strain–displacement relation and the method of partial integration, u_r may be expressed as

$$\begin{aligned}u_r &= \int\varepsilon_r\mathrm{d}r=\int\frac{K(z,r)}{4E\sqrt{2\pi r}}\left((5-3v-8vT_z(r,z))\cos\frac{\theta}{2}-(1+v)\cos\frac{3}{2}\theta\right)\mathrm{d}r\\ &= \frac{\left((5-3v)\cos\frac{\theta}{2}-(1+v)\cos\frac{3}{2}\theta\right)}{4\sqrt{2\pi}E}\int\frac{K}{\sqrt{r}}\mathrm{d}r-\frac{2v\cos\frac{\theta}{2}}{\sqrt{2\pi}E}\int\frac{T_zK}{\sqrt{r}}\mathrm{d}r,\\ &= \frac{\left((5-3v)\cos\frac{\theta}{2}-(1+v)\cos\frac{3}{2}\theta\right)}{2\sqrt{2\pi}E}\left(K\sqrt{r}-\int(K)'\sqrt{r}\mathrm{d}r\right)\\ &\quad-\frac{4v}{\sqrt{2\pi}E}\cos\frac{\theta}{2}\left(T_zK\sqrt{r}-\int(T_zK)'\sqrt{r}\mathrm{d}r\right)\\ &\approx \frac{K(z,r)\sqrt{r}}{2\sqrt{2\pi}E}\left((5-3v-8vT_z(z,r))\cos\frac{1}{2}\theta-(1+v)\cos\frac{3}{2}\theta\right).\end{aligned} \tag{26}$$

Here, $\int(K)'\sqrt{r}\mathrm{d}r$ and $\int(T_zK)'\sqrt{r}\mathrm{d}r$ are ignored because of the following equations:

$$\begin{aligned}\lim_{r\to0}\frac{\int(K)'\sqrt{r}\mathrm{d}(r)}{K\sqrt{r}} &= \frac{(K)'r}{(K)'r+\frac{1}{2}K}=0,\\ \lim_{r\to0}\frac{\int(T_zK)'\sqrt{r}\mathrm{d}(r)}{T_zK\sqrt{r}} &= \frac{(T_zK)'r}{(T_zK)'r+\frac{1}{2}T_zK}=0.\end{aligned} \tag{27}$$

Considering the strain–displacement relations, one may have the expressions of $(u_r)^{\cdot}$, $(u_\theta)^{\cdot}$, and u_θ, as

$$\begin{aligned}(u_r)^{\cdot} &= \frac{K(z,r)\sqrt{r}}{4\sqrt{2\pi}E}\left(-(5-3v-8vT_z(z,r))\sin\frac{\theta}{2}+3(1+v)\sin\frac{3}{2}\theta\right),\\ (u_\theta)^{\cdot} &= \varepsilon_\theta r-u_r=\frac{K(z,r)\sqrt{r}}{4\sqrt{2\pi}E}\left((-7+v+8vT_z(z,r))\cos\frac{\theta}{2}+3(1+v)\cos\frac{3}{2}\theta\right),\\ u_\theta &= \frac{K(z,r)\sqrt{r}}{2\sqrt{2\pi}E}\left((-7+v+8vT_z(z,r))\sin\frac{\theta}{2}+(1+v)\sin\frac{3}{2}\theta\right).\end{aligned} \tag{28}$$

Substituting Eqs. (18), (26), and (28) into Eq. (25), one may have

$$
\begin{aligned}
-\int_{\Gamma_1} \sigma_{ij} n_j u_{i,x} \mathrm{d}s = & -\frac{K^2(z,r)}{32\pi E} \int_{-\pi}^{\pi} \left(5\cos\frac{1}{2}\theta - \cos\frac{3}{2}\theta\right) \Big\{ -(9+v-8vT_z(z,r))\sin\frac{1}{2}\theta\sin\theta \\
& -(1+v)\sin\frac{3}{2}\theta\sin\theta + (5-3v-8vT_z(z,r))\cos\frac{1}{2}\theta\cos\theta - (1+v)\cos\frac{3}{2}\theta\cos\theta \Big\} \mathrm{d}\theta \\
& -\frac{K^2(z,r)}{32\pi E} \int_{-\pi}^{\pi} \left(\sin\frac{1}{2}\theta + \sin\frac{3}{2}\theta\right) \Big\{ -(3-5v-8vT_z(z,r))\cos\frac{1}{2}\theta\sin\theta \\
& -(1+v)\cos\frac{3}{2}\theta\sin\theta - (7-v-8vT_z(z,r))\sin\frac{1}{2}\theta\cos\theta + (1+v)\sin\frac{3}{2}\theta\cos\theta \Big\} \mathrm{d}\theta \\
= & -\frac{K^2(z,r)}{4E}(2vT_z(z,r) - v - 3). \qquad (29)
\end{aligned}
$$

Substituting Eqs. (24) and (29) into Eq. (22), one may have

$$
\begin{aligned}
J(z) &= \int_{\Gamma_1} \left(W\mathrm{d}y - \sigma_{ij} n_j u_{i,x} \mathrm{d}s\right) = \frac{K^2(z,r)}{2E}\left((T_z(z,r))^2 - 3vT_z(z,r) + 2\right) \\
&\text{or} \\
K(z,r) &= \sqrt{\frac{2EJ(z)}{(T_z(z,r))^2 - 3vT_z(z,r) + 2}}. \qquad (30)
\end{aligned}
$$

Specially, $K = \sqrt{EJ}$ when $T_z = 0$ (plane stress), and $K = \sqrt{\frac{EJ}{1-v^2}}$ when $T_z = v$ (plane strain).

4 Three-dimensional finite element model

$K(z,r)$ is undetermined and should be related to the applied loading. On the other hand, Eq. (30) shows that $K(z,r)$ depends on $J(z)$ and $T_z(z,r)$. When the values of $J(z)$ and $T_z(z,r)$ are determined by three-dimensional finite element methods, the value of $K(z,r)$ can be obtained by Eq. (30).

A cylinder containing a crack front is considered, see Fig. 3a. Considering symmetry conditions in the problem, only a quarter of the cylinder is modeled, and the mesh is constructed with 8-node three-dimensional brick elements, as shown in Fig. 3b. In x–y planes, the size of an element increases progressively in the radial direction, and the progression ratio is taken as 1.21. All radial sizes of the elements at the crack front are $2 \times 10^{-5}h$, while there are 36 elements which distribute uniformly in the circumferential direction. The same planar mesh is repeated along the z-axis from the mid-plane ($z = 0$) to the free surface ($z = h$). There are sixty elements along the crack front, and the thickness of an element increases gradually when approaching the mid-plane. The progression ratio is 1.12, and the minimum thickness of elements at the free surface is $1.11 \times 10^{-4}h$.

Boundary conditions for the current problem may be expressed as

$$
\begin{aligned}
u_z|_{z=0} &= 0, u_y\big|_{y=0,x\geq 0} = 0, \\
\sigma_r|_{r=a} &= \frac{K^{\mathrm{far}}}{4\sqrt{2\pi a}}\left(5\cos\frac{\theta}{2} - \cos\frac{3}{2}\theta\right), \\
\sigma_{r\theta}|_{r=a} &= \frac{K^{\mathrm{far}}}{4\sqrt{2\pi a}}\left(\sin\frac{\theta}{2} + \sin\frac{3}{2}\theta\right). \qquad (31)
\end{aligned}
$$

Here, $K^{\mathrm{far}} = \sqrt{2\pi a}\sigma^{\infty}$, and $a = 10h$.

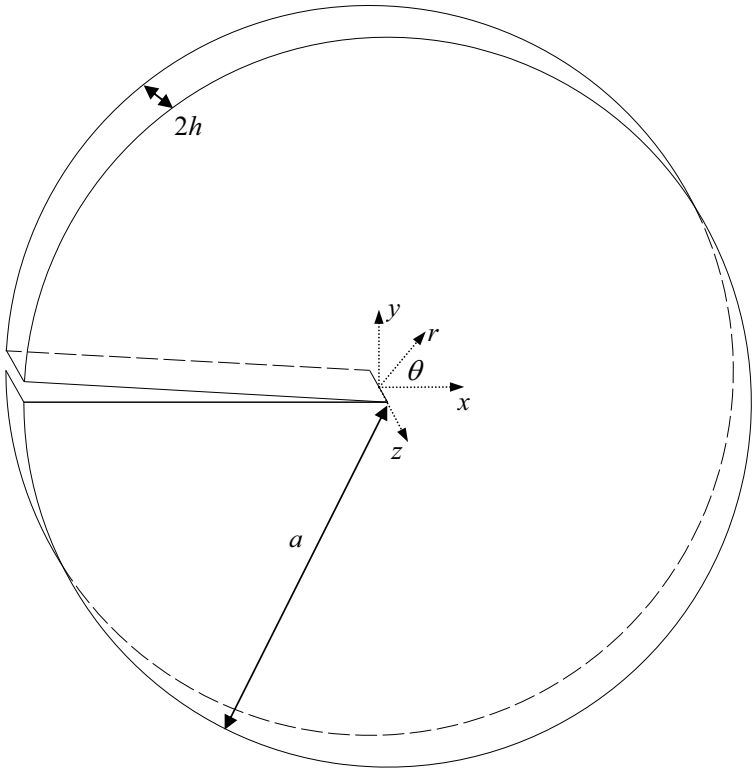

(a)

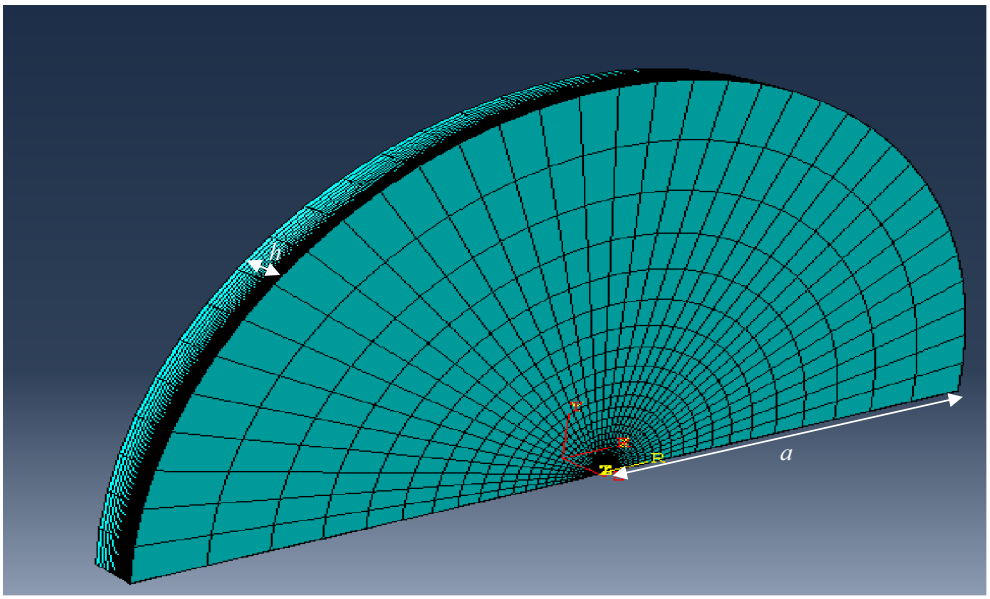

(b)

Fig. 3 **a** A cracked cylinder containing a crack front, **b** finite element mesh of the quarter-mode. Here, $a = 10h$

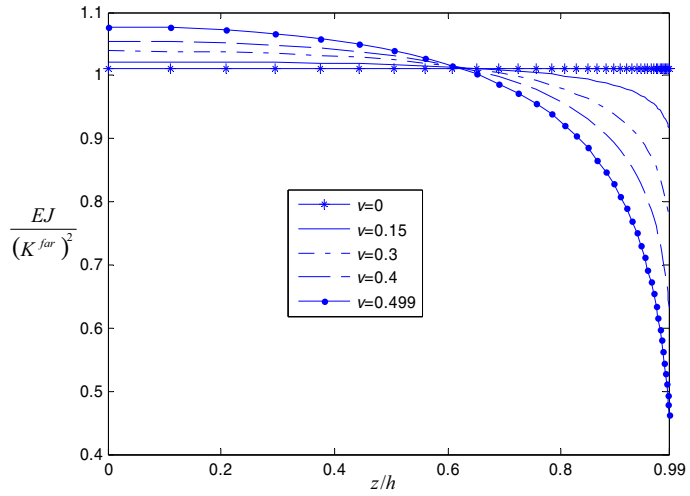

(a)

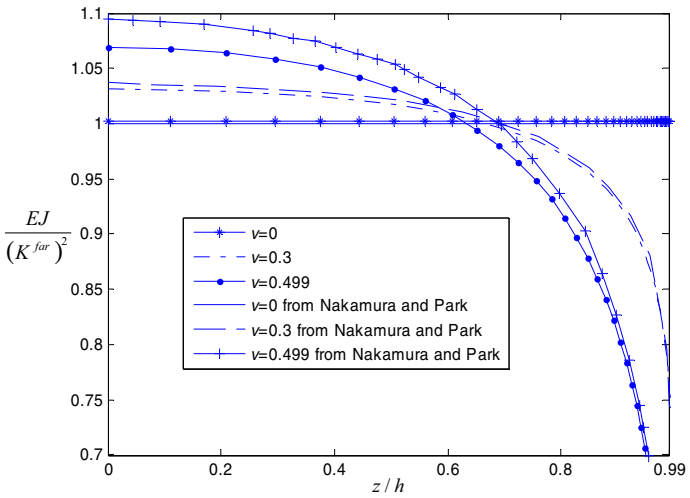

(b)

Fig. 4 **a** $\frac{J}{(K^{\text{far}})^2}$ along the half-crack front for various Poisson's ratios, **b** comparison with Nakamura and Park's results

5 Results and discussions

Figure 4a shows that the value of $J(z)$ decreases from the mid-plane ($z = 0$) to the plane near the free surface ($z = 0.99$). Figure 4b shows that the current results are in good agreement with the results given by Nakamura and Parks [7]. Based on the current numerical results, a fitting equation for $J(z)$ may be expressed as

$$\frac{EJ}{\left(K^{\text{far}}\right)^2} = \frac{P_1 \frac{z}{h} + P_2}{\frac{z}{h} + P_3}, 0 \le \frac{z}{h} \le 0.99. \tag{32}$$

The coefficients P_1, P_2, and P_3 for various Poisson's ratios are shown in Table 1.

The variation of $\frac{T_z}{v}$ in the radial direction near the crack front for various normalized depth z/h is plotted in Fig. 5. One may observe that when r tends to zero, the value of T_z tends to v for a normalized depth which varies from 0 to 0.99. This may imply that plane strain conditions can be met when r is zero except at the corner point. Figure 5 also illustrates that the value of T_z decreases with increasing r, and the three-dimensional effect appears within a radial distance of about one half of the plate thickness from the crack front in the mid-plane.

Table 1 The values of P_1, P_2, and P_3 for various Poisson's ratios

v	P_1	P_2	P_3
0	1	− 1	− 1
0.15	1.028	− 1.074	− 1.051
0.3	1.055	− 1.096	− 1.057
0.4	1.084	− 1.120	− 1.062
0.499	1.127	− 1.155	− 1.071

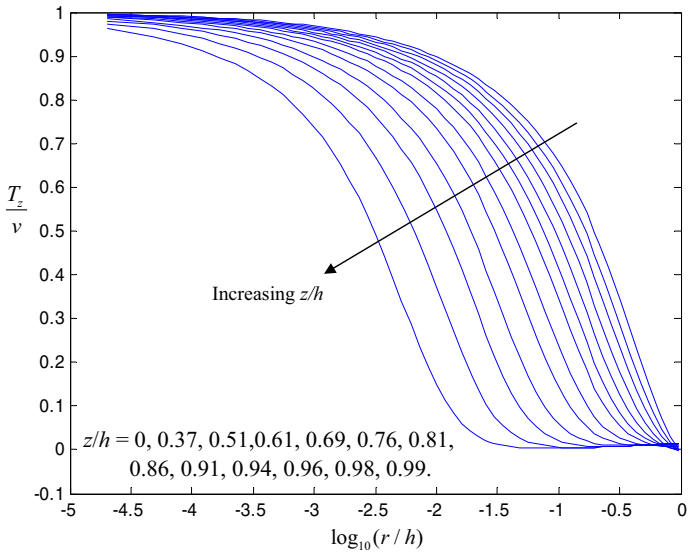

Fig. 5 The variation of $\frac{T_z}{v}$ in the radial direction near the half-crack front for various depths

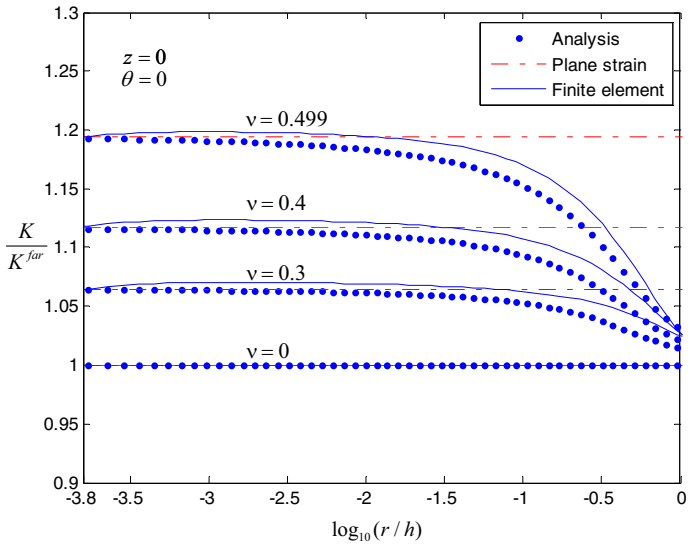

Fig. 6 The variation of $\frac{K}{K^{far}}$ in the radial direction for various Poisson's ratios. Here, the analytical results are given by Eq. (30), the numerical results are given by $K = \sigma_y\sqrt{2\pi r}$, and the plane strain K-field results are given by $K = \sqrt{\frac{EJ(z)}{1-v^2}}$

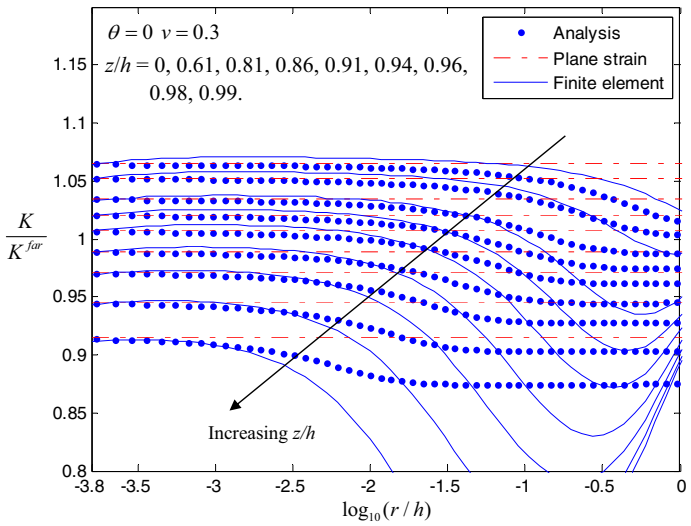

(a)

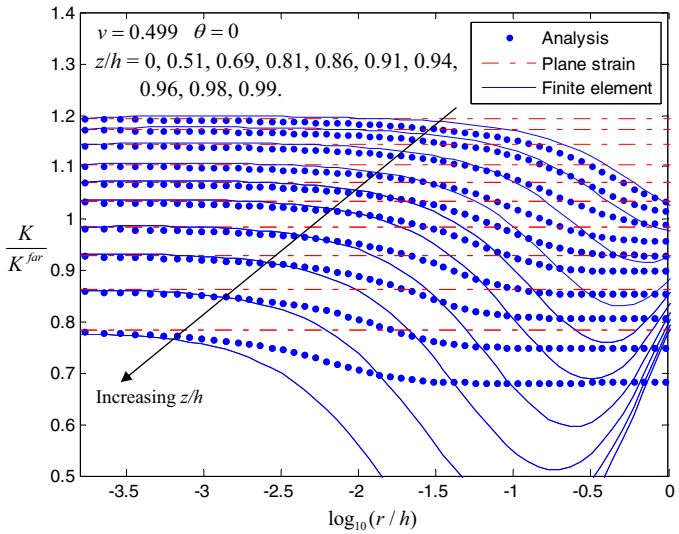

(b)

Fig. 7 The variation of $\frac{K}{K^{\text{far}}}$ in the radial direction for various depths. Here, the analytical results are given by Eq. (30), the numerical results are given by $K = \sigma_y\sqrt{2\pi r}$, and the plane strain K-field results are given by $K = \sqrt{\frac{EJ(z)}{1-\nu^2}}$

The value of T_z decreases more quickly with increasing normalized depth z/h, and T_z vanishes at a radial distance of about 1.5% of the plate thickness from the crack front when z/h is 0.99. Based on the numerical results in Fig. 5, a fitting equation for T_z may be expressed by

$$\frac{T_z}{v} = \frac{q_1\left(\frac{r}{h}\right)^3 + q_2\left(\frac{r}{h}\right)^2 + q_3\frac{r}{h} + q_4}{\frac{r}{h} + q_4},$$

$$q_1 = 32.5\left(\frac{z}{h}\right)^5 - 57.25\left(\frac{z}{h}\right)^4 + 21.7\left(\frac{z}{h}\right)^3 + 3.658\left(\frac{z}{h}\right)^2 - 1.875\frac{z}{h} + 0.939,$$

$$q_2 = -49.35\left(\frac{z}{h}\right)^5 + 85.57\left(\frac{z}{h}\right)^4 - 34.71\left(\frac{z}{h}\right)^3 - 1.319\left(\frac{z}{h}\right)^2 + 1.845\frac{z}{h} - 1.697,$$

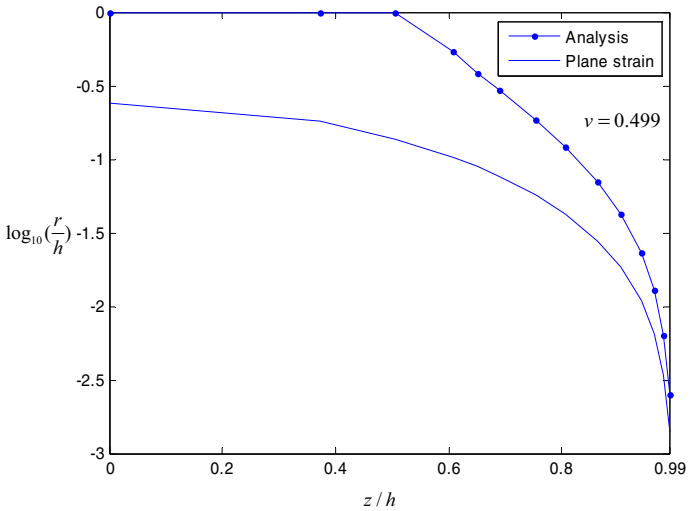

Fig. 8 The variation of the radii of effective regions for analytical solutions and plane strain solutions in the thickness direction

$$q_3 = 14.79\left(\frac{z}{h}\right)^5 - 20.14\left(\frac{z}{h}\right)^4 + 2.504\left(\frac{z}{h}\right)^3 + 2.944\left(\frac{z}{h}\right)^2 - 0.893\frac{z}{h} + 0.762,$$
$$q_4 = 14.56\left(\frac{z}{h}\right)^6 - 42.48\left(\frac{z}{h}\right)^5 + 44.49\left(\frac{z}{h}\right)^4 - 20.26\left(\frac{z}{h}\right)^3 + 3.87\left(\frac{z}{h}\right)^2 - 0.2\frac{z}{h} + 0.019,$$
$$0 \le \frac{r}{h} \le 1, 0 \le \frac{z}{h}0 \le 0.99. \tag{33}$$

The variations of $\frac{K(z,r)}{K^{\text{far}}}$ in the radial direction in the mid-plane for various Poisson's ratios are plotted in Fig. 6. In this Figure, the analytical results of $K(z,r)$ are given by Eq. (30), the numerical results of $K(z,r)$ are given by the equation that $K(z,r) = \sigma_y\sqrt{2\pi r}$, and the plane strain K-field results are given by the equation that $K(z,r) = \sqrt{\frac{EJ(z)}{1-v^2}}$. From Fig. 6, one may observe that the analytical results agree with the corresponding numerical results. Both analytical and numerical results show that the value of $\frac{K(z,r)}{K^{\text{far}}}$ decreases with increasing r. This may imply that the value of $\frac{K(z,r)}{K^{\text{far}}}$ decreases with decreasing T_z. Figure 6 also shows that when r tends to zero, both analytical and numerical results tend to the corresponding plane strain K-field results. However, the difference between the numerical results and the corresponding plane strain K-field results becomes larger with increasing r. In the case that $v \le 0.3$, the maximum deviation from the numerical results, measured by $\left|\left(\sigma_y\sqrt{2\pi r} - \sqrt{\frac{EJ(z)}{1-v^2}}\right)/\sigma_y\sqrt{2\pi r}\right|$, is less than 5%. So, in this case the plane strain K-field solutions are accurate enough to depict the stress state in the region $0 < r/h < 1$ in the mid-plane. But when Poisson's ratio has a larger value, for example, it is taken as 0.499, the maximum deviation reaches 17%, which should not be ignored.

The variation of $\frac{K(z,r)}{K^{\text{far}}}$ in the radial direction for various normalized depths z/h is depicted in Fig. 7. This Figure shows that the analytical results, the plane strain K-field results, and the numerical results are consistent in the region close to the crack front. However, the radius of the region becomes smaller when approaching the free surface. In the plane which is very close to the free surface ($z/h = 0.99$), the radius is about $10^{-3}\ h$.

Based on a criterion that $\left|\left(\sigma_y\sqrt{2\pi r} - \sqrt{\frac{2EJ}{(T_z)^2-3vT_z+2}}\right)/\sigma_y\sqrt{2\pi r}\right| \le 5\%$ or $\left|\left(\sigma_y\sqrt{2\pi r} - \sqrt{\frac{EJ(z)}{1-v^2}}\right)/\sigma_y\sqrt{2\pi r}\right| \le 5\%$, the radius of the region where the analytical results or the plane strain K-field results can match the numerical results is plotted in Fig. 8. The Figure shows that the current analytical results are effective in a larger region than the corresponding plane strain K-field results.

In comparison with numerical results, fitting results for $\frac{EJ}{(K^{\text{far}})^2}$ and $\frac{T_z}{v}$ match the corresponding numerical results, as shown in Fig. 9.

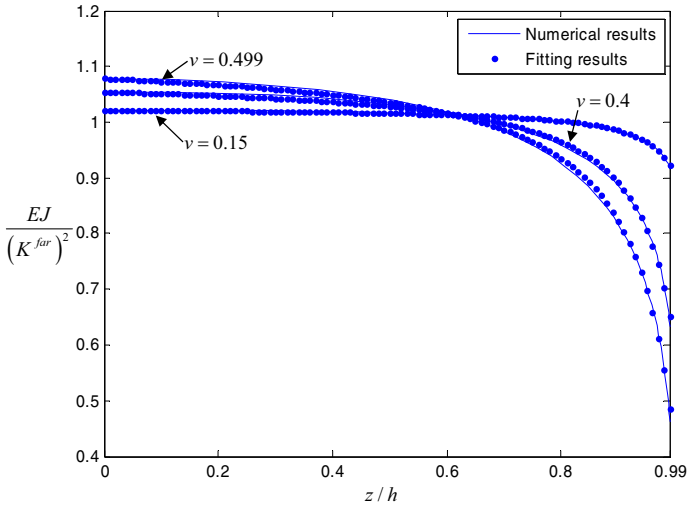

Fig. 9 Comparison of fitting results with corresponding numerical results; **a** $\frac{EJ}{(K^{\text{far}})^2}$, **b** $\frac{T_z}{\nu}$

6 Summary and conclusions

Considering a thin elastic plate containing a through-thickness crack under tension, we propose an analytical solution for the three-dimensional singularity fields in the region where the gradual transition from plane strain conditions to plane stress conditions occurs. Three-dimensional Maxwell stress functions, the principle of minimum complementary potential energy, and three-dimensional J-integrals are employed to derive the field equations near the crack front. Three-dimensional finite element simulations with fine meshes are carried out to verify the analytical solutions. A comparison with numerical results shows that the current analytical results are effective. Based on the current numerical results, two fitting equations for $J(z)$ and T_z are given in Eqs. (32) and (33) for possible practical applications.

This work supports the following observations and conclusions:

(i) Plane strain conditions can be met at the crack front except the corner point.
(ii) The three-dimensional effect appears within a radial distance of about one half of the plate thickness from the crack front in the mid-plane. But, the radial distance becomes smaller when approaching the free

surface. In the plane very close to the free surface($z/h = 0.99$), the radial distance is about 1.5% of the plate thickness.

(iii) When r tends to zero, analytical and numerical results for $K(z, r)$ tend to the corresponding plane strain K-field results. However, both analytical and numerical results show that the value of $K(z, r)$ decreases with increasing r, or decreasing T_z. If Poisson's ratio is less than 0.3, the difference between numerical results and the corresponding plane strain K-field results may be ignored. But if Poisson's ratio is taken a larger value, such as 0.499, the maximum deviation from the numerical results is up to 17%.

(iv) Compared with plane strain K-field solutions, the current analytical solutions for crack front fields can be applied in a larger region.

Appendix

According to the principle of minimum complementary potential energy, one may have

$$\iiint_V \left(\varepsilon_x \delta\sigma_x + \varepsilon_y \delta\sigma_y + \varepsilon_z \delta\sigma_z + \gamma_{xy}\delta\sigma_{xy} + \gamma_{xz}\delta\sigma_{xz} + \gamma_{yz}\delta\sigma_{yz}\right) \mathrm{d}x\mathrm{d}y\mathrm{d}z = 0. \tag{A.1}$$

Stress components related to three-dimensional Maxwell functions in a rectilinear coordinate system may be expressed as

$$\begin{aligned} &\sigma_x = \frac{\partial^2\phi_2}{\partial z^2} + \frac{\partial^2\phi_3}{\partial y^2}, \sigma_y = \frac{\partial^2\phi_1}{\partial z^2} + \frac{\partial^2\phi_3}{\partial x^2}, \sigma_z = \frac{\partial^2\phi_1}{\partial y^2} + \frac{\partial^2\phi_2}{\partial x^2}, \\ &\sigma_{xy} = -\frac{\partial^2\phi_3}{\partial x\partial y}, \sigma_{xz} = -\frac{\partial^2\phi_2}{\partial x\partial z}, \sigma_{yz} = -\frac{\partial^2\phi_1}{\partial y\partial z}. \end{aligned} \tag{A.2}$$

Substituting Eq. (A.2) into Eq. (A.1) , one may have

$$\begin{aligned} \iiint_V \Bigg[&\varepsilon_x \delta\left(\frac{\partial^2\phi_2}{\partial z^2} + \frac{\partial^2\phi_3}{\partial y^2}\right) + \varepsilon_y \delta\left(\frac{\partial^2\phi_1}{\partial z^2} + \frac{\partial^2\phi_3}{\partial x^2}\right) + \varepsilon_z \delta\left(\frac{\partial^2\phi_1}{\partial y^2} + \frac{\partial^2\phi_2}{\partial x^2}\right) \\ &-\gamma_{xy}\frac{\partial^2\delta\phi_3}{\partial x\partial y} - \gamma_{xz}\frac{\partial^2\phi_2}{\partial x\partial z} - \gamma_{yz}\frac{\partial^2\phi_1}{\partial y\partial z}\Bigg] \mathrm{d}x\mathrm{d}y\mathrm{d}z = 0. \end{aligned} \tag{A.3}$$

According to derivation rules, one may have

$$\begin{aligned} \varepsilon_x \delta\left(\frac{\partial^2\phi_2}{\partial z^2} + \frac{\partial^2\phi_3}{\partial y^2}\right) &= \frac{\partial}{\partial z}\left(\varepsilon_x \frac{\partial(\delta\phi_2)}{\partial z} - \frac{\partial\varepsilon_x}{\partial z}\delta\phi_2\right) + \frac{\partial^2(\varepsilon_x)}{\partial z^2}\delta\phi_2 + \frac{\partial}{\partial y}\left(\varepsilon_x \frac{\partial(\delta\phi_3)}{\partial y} - \frac{\partial\varepsilon_x}{\partial y}\delta\phi_3\right) \\ &\quad + \frac{\partial^2(\varepsilon_x)}{\partial y^2}\delta\phi_3, \\ \varepsilon_y \delta\left(\frac{\partial^2\phi_1}{\partial z^2} + \frac{\partial^2\phi_3}{\partial x^2}\right) &= \frac{\partial}{\partial z}\left(\varepsilon_y \frac{\partial(\delta\phi_1)}{\partial z} - \frac{\partial\varepsilon_y}{\partial z}\delta\phi_1\right) + \frac{\partial^2(\varepsilon_y)}{\partial z^2}\delta\phi_1 + \frac{\partial}{\partial x}\left(\varepsilon_y \frac{\partial(\delta\phi_3)}{\partial x} - \frac{\partial\varepsilon_y}{\partial x}\delta\phi_3\right) \\ &\quad + \frac{\partial^2(\varepsilon_y)}{\partial x^2}\delta\phi_3, \\ \varepsilon_z \delta\left(\frac{\partial^2\phi_1}{\partial y^2} + \frac{\partial^2\phi_2}{\partial x^2}\right) &= \frac{\partial}{\partial y}\left(\varepsilon_z \frac{\partial(\delta\phi_1)}{\partial y} - \frac{\partial\varepsilon_z}{\partial y}\delta\phi_1\right) + \frac{\partial^2(\varepsilon_z)}{\partial y^2}\delta\phi_1 + \frac{\partial}{\partial x}\left(\varepsilon_z \frac{\partial(\delta\phi_2)}{\partial x} - \frac{\partial\varepsilon_z}{\partial x}\delta\phi_2\right) \\ &\quad + \frac{\partial^2(\varepsilon_z)}{\partial x^2}\delta\phi_2, \\ -\gamma_{xy}\frac{\partial^2(\delta\phi_3)}{\partial x\partial y} &= -\frac{\partial\left(\gamma_{xy}\frac{\partial}{\partial y}\delta\phi_3\right)}{\partial x} + \frac{\partial}{\partial y}\left(\frac{\partial\gamma_{xy}}{\partial x}\delta\phi_3\right) - \frac{\partial^2(\gamma_{xy})}{\partial y\partial x}\delta\phi_3, \end{aligned}$$

$$-\gamma_{xz}\frac{\partial^2(\phi_2)}{\partial x\partial z}=-\frac{\partial\left(\gamma_{xz}\frac{\partial}{\partial z}\delta\phi_2\right)}{\partial x}+\frac{\partial}{\partial z}\left(\frac{\partial\gamma_{xz}}{\partial x}\delta\phi_2\right)-\frac{\partial^2(\gamma_{xz})}{\partial z\partial x}\delta\phi_2,$$
$$-\gamma_{yz}\frac{\partial^2(\phi_1)}{\partial y\partial z}=-\frac{\partial\left(\gamma_{yz}\frac{\partial}{\partial z}\delta\phi_1\right)}{\partial y}+\frac{\partial}{\partial z}\left(\frac{\partial\gamma_{yz}}{\partial y}\delta\phi_1\right)-\frac{\partial^2(\gamma_{yz})}{\partial z\partial y}\delta\phi_1. \tag{A.4}$$

Substituting Eq. (A.4) into Eqs. (A.3), (A.3) may be re-written as

$$\begin{aligned}
&\iiint_V\frac{\partial}{\partial x}\left(-\frac{\partial\varepsilon_z}{\partial x}\delta\phi_2-\frac{\partial\varepsilon_y}{\partial x}\delta\phi_3+\varepsilon_z\frac{\partial(\delta\phi_2)}{\partial x}-\gamma_{xz}\frac{\partial(\delta\phi_2)}{\partial z}+\varepsilon_y\frac{\partial(\delta\phi_3)}{\partial x}-\gamma_{xy}\frac{\partial(\delta\phi_3)}{\partial y}\right)\mathrm{d}x\mathrm{d}y\mathrm{d}z\\
&+\iiint_V\frac{\partial}{\partial y}\left(-\frac{\partial\varepsilon_z}{\partial y}\delta\phi_1+\left(\frac{\partial\gamma_{xy}}{\partial x}-\frac{\partial\varepsilon_x}{\partial y}\right)\delta\phi_3+\varepsilon_z\frac{\partial(\delta\phi_1)}{\partial y}-\gamma_{yz}\frac{\partial(\delta\phi_1)}{\partial z}+\varepsilon_x\frac{\partial(\delta\phi_3)}{\partial y}\right)\mathrm{d}x\mathrm{d}y\mathrm{d}z\\
&+\iiint_V\frac{\partial}{\partial z}\left(\left(\frac{\partial\gamma_{yz}}{\partial y}-\frac{\partial\varepsilon_y}{\partial z}\right)\delta\phi_1+\left(\frac{\partial\gamma_{xz}}{\partial x}-\frac{\partial\varepsilon_x}{\partial z}\right)\delta\phi_2+\varepsilon_y\frac{\partial(\delta\phi_1)}{\partial z}+\varepsilon_x\frac{\partial(\delta\phi_2)}{\partial z}\right)\mathrm{d}x\mathrm{d}y\mathrm{d}z\\
&+\iiint_V\left[\left(\frac{\partial^2(\varepsilon_z)}{\partial y^2}+\frac{\partial^2(\varepsilon_y)}{\partial z^2}-\frac{\partial^2\gamma_{yz}}{\partial z\partial y}\right)\delta\phi_1+\left(\frac{\partial^2(\varepsilon_z)}{\partial x^2}+\frac{\partial^2(\varepsilon_x)}{\partial z^2}-\frac{\partial^2\gamma_{xz}}{\partial z\partial x}\right)\delta\phi_2\right.\\
&\left.+\left(\frac{\partial^2(\varepsilon_y)}{\partial x^2}+\frac{\partial^2(\varepsilon_x)}{\partial y^2}-\frac{\partial^2\gamma_{xy}}{\partial y\partial x}\right)\delta\phi_3\right]\mathrm{d}x\mathrm{d}y\mathrm{d}z=0.
\end{aligned}\tag{A.5}$$

Equation (A.5) may be re-written as

$$\begin{aligned}
&\iint_{S_1}\left(-\frac{\partial\varepsilon_z}{\partial x}\delta\phi_2-\frac{\partial\varepsilon_y}{\partial x}\delta\phi_3+\varepsilon_z\frac{\partial(\delta\phi_2)}{\partial x}-\gamma_{xz}\frac{\partial(\delta\phi_2)}{\partial z}+\varepsilon_y\frac{\partial(\delta\phi_3)}{\partial x}-\gamma_{xy}\frac{\partial(\delta\phi_3)}{\partial y}\right)\mathrm{d}y\mathrm{d}z\\
&+\iint_{S_2}\left(-\frac{\partial\varepsilon_z}{\partial y}\delta\phi_1+\left(\frac{\partial\gamma_{xy}}{\partial x}-\frac{\partial\varepsilon_x}{\partial y}\right)\delta\phi_3+\varepsilon_z\frac{\partial(\delta\phi_1)}{\partial y}-\gamma_{yz}\frac{\partial(\delta\phi_1)}{\partial z}+\varepsilon_x\frac{\partial(\delta\phi_3)}{\partial y}\right)\mathrm{d}x\mathrm{d}z\\
&+\iint_{S_3}\left(\frac{\partial\gamma_{yz}}{\partial y}-\frac{\partial\varepsilon_y}{\partial z}\right)\delta\phi_1+\left(\frac{\partial\gamma_{xz}}{\partial x}-\frac{\partial\varepsilon_x}{\partial z}\right)\delta\phi_2+\varepsilon_y\frac{\partial(\delta\phi_1)}{\partial z}+\varepsilon_x\frac{\partial(\delta\phi_2)}{\partial z}\mathrm{d}x\mathrm{d}y\\
&\iiint_V\left[\left(\frac{\partial^2(\varepsilon_z)}{\partial y^2}+\frac{\partial^2(\varepsilon_y)}{\partial z^2}-\frac{\partial^2(\gamma_{yz})}{\partial z\partial y}\right)\delta\phi_1+\left(\frac{\partial^2(\varepsilon_z)}{\partial x^2}+\frac{\partial^2(\varepsilon_x)}{\partial z^2}-\frac{\partial^2(\gamma_{xz})}{\partial z\partial x}\right)\delta\phi_2\right.\\
&\left.+\left(\frac{\partial^2(\varepsilon_y)}{\partial x^2}+\frac{\partial^2(\varepsilon_x)}{\partial y^2}-\frac{\partial^2(\gamma_{xy})}{\partial y\partial x}\right)\delta\phi_3\right]\mathrm{d}x\mathrm{d}y\mathrm{d}z=0.
\end{aligned}\tag{A.6}$$

Considering compatibility equations, the last integral in Eq. (A.6) should be zero. Furthermore, considering $\phi_1=\phi_2$and $\phi_3=\phi$, one may have

$$\begin{aligned}
&\iiint_V\left[\left(\frac{\partial^2(\varepsilon_z)}{\partial x^2}+\frac{\partial^2(\varepsilon_z)}{\partial y^2}-\frac{\partial^2(\gamma_{xz})}{\partial z\partial x}-\frac{\partial^2(\gamma_{yz})}{\partial z\partial y}+\frac{\partial^2(\varepsilon_x)}{\partial z^2}+\frac{\partial^2(\varepsilon_y)}{\partial z^2}\right)\delta\phi_1\right.\\
&\left.+\left(\frac{\partial^2(\varepsilon_y)}{\partial x^2}+\frac{\partial^2(\varepsilon_x)}{\partial y^2}-\frac{\partial^2(\gamma_{xy})}{\partial y\partial x}\right)\delta\phi\right]\mathrm{d}x\mathrm{d}y\mathrm{d}z=0.
\end{aligned}\tag{A.7}$$

Ignoring higher terms of r and using cylindrical coordinates r, θ, and z, Eq. (A.7) may be re-written as

$$\iiint_V\left[\left(\frac{\partial^2(\varepsilon_z)}{\partial x^2}+\frac{\partial^2(\varepsilon_z)}{\partial y^2}-\frac{\partial^2(\gamma_{xz})}{\partial z\partial x}-\frac{\partial^2(\gamma_{yz})}{\partial z\partial y}+\frac{\partial^2(\varepsilon_x)}{\partial z^2}+\frac{\partial^2(\varepsilon_y)}{\partial z^2}\right)\delta\phi_1\right.$$

$$
\begin{aligned}
&+\left(\frac{\partial^2\left(\varepsilon_y\right)}{\partial x^2}+\frac{\partial^2\left(\varepsilon_x\right)}{\partial y^2}-\frac{\partial^2\left(\gamma_{xy}\right)}{\partial y\partial x}\right)\Bigg]\delta\phi\mathrm{d}x\mathrm{d}y\mathrm{d}z\\
&\approx\iiint_V\left[\left(\frac{\partial^2\left(\varepsilon_z\right)}{\partial x^2}+\frac{\partial^2\left(\varepsilon_z\right)}{\partial y^2}\right)\delta\phi_1+\left(\frac{\partial^2\left(\varepsilon_y\right)}{\partial x^2}+\frac{\partial^2\left(\varepsilon_x\right)}{\partial y^2}-\frac{\partial^2\left(\gamma_{xy}\right)}{\partial y\partial x}\right)\delta\phi\right]\mathrm{d}x\mathrm{d}y\mathrm{d}z\\
&=\iiint_V\left[\left(\frac{1}{r}\left(\varepsilon_z\right)^{\cdot\cdot}+\left(\varepsilon_z r\right)^{\prime\prime}-\left(\varepsilon_z\right)^{\prime}\right)\delta\phi_1\right.\\
&\left.+\left(\left(r\varepsilon_\theta\right)^{\prime\prime}+\frac{\left(\varepsilon_r\right)^{\cdot\cdot}}{r}-\left(\varepsilon_r\right)^{\prime}-\left(\gamma_{r\theta}\right)^{\cdot\prime}-\left(\frac{\gamma_{r\theta}}{r}\right)^{\cdot}\right)\delta\phi\right]r\mathrm{d}r\mathrm{d}\theta\mathrm{d}z=0.
\end{aligned}
\tag{A.8}
$$

Considering that $\delta\phi$ and $\delta\phi_1$ are arbitrary, one may have

$$
\begin{aligned}
&\left(r\varepsilon_\theta\right)^{\prime\prime}+\frac{\left(\varepsilon_r\right)^{\cdot\cdot}}{r}-\left(\varepsilon_r\right)^{\prime}-\left(\gamma_{r\theta}\right)^{\cdot\prime}-\left(\frac{\gamma_{r\theta}}{r}\right)^{\cdot}=0,\\
&\left(r\varepsilon_z\right)^{\prime\prime}+\left(\frac{\varepsilon_z}{r}\right)^{\cdot\cdot}-\left(\varepsilon_z\right)^{\prime}=0.
\end{aligned}
\tag{A.9}
$$

References

1. Anderson, T.L.: Fracture Mechanics: Fundamentals and Applications, 3rd edn. CRC Press, Boca Raton (2005)
2. Hartranft, R., Sih, G.C.: An approximate three-dimensional theory of plates with application to crack problems. Int. J. Eng. Sci. **8**, 711–729 (1970)
3. Sih, G.C.: A review of the three-dimensional stress problem for a cracked plate. Int. J. Fract. Mech. **7**, 39–61 (1971)
4. Benthem, J.P.: State of stress at the vertex of a quarter-infinite crack in a half-space. Int. J. Solids Struct. **13**, 479–492 (1977)
5. Kawai, T., Fujitani, Y., Kumagai, K.: Analysis of singularity at the root of the surface crack problem. In: Proceedings of the International Conference on Fracture Mechanics and Technology. Hong Kong, China (1977)
6. Yang, W., Freund, L.B.: Transverse shear effects for through-cracks in an elastic plate. Int. J. Solids Struct. **21**, 977–994 (1985)
7. Nakamura, T., Parks, D.M.: Three-dimensional stress field near the crack front of a thin elastic plate. J. Appl. Mech. **55**, 805–813 (1988)
8. Pook, L.P.: A note on corner point singularities. Int. J. Fract. **53**, R3–R8 (1992)
9. Pook, L.P.: Some implications of corner point singularities. Eng. Fract. Mech. **48**, 367–378 (1994)
10. Pook, L.P.: On fatigue crack paths. Int. J. Fatigue **17**, 5–13 (1995)
11. Leung, A., Su, R.: Analytical solution for mode I crack orthogonal to free surface. Int. J. Fract. **76**, 79–95 (1996)
12. Kwon, S.W., Sun, C.T.: Characteristics of three-dimensional stress fields in plates with a through-the-thickness crack. Int. J. Fract. **104**, 291–315 (2000)
13. Noda, N.: Stress intensity formulas for three-dimensional cracks in homogeneous and bonded dissimilar materials. Eng. Fract. Mech. **71**, 1–15 (2004)
14. Kotousov, A.: Fracture in plates of finite thickness. Int. J. Solids Struct. **44**, 8259–8273 (2007)
15. Luo, J., Wang, X.: On the anti-plane shear of an elliptic nano inhomogeneity. Eur. J. Mech. A Solids **28**, 926–934 (2009)
16. Hutar, P., Nahlik, L., Knesl, Z.: The effect of a free surface on fatigue crack behavior. Int. J. Fatigue **32**, 1265–1269 (2010)
17. Kotousov, A., Lazzarin, P., Berto, F., Pook, L.P.: Three-dimensional stress states at crack tip induced by shear and anti-plane loading. Eng. Fract. Mech. **108**, 65–74 (2013)
18. Zhou, K., Wei, R.: Modeling cracks and inclusions near surfaces under contact loading. Int. J. Mech. Sci. **83**, 163–171 (2014)
19. Zhou, K., Wei, R.: Semi-analytic solution of multiple inhomogeneous inclusions and cracks in an infinite space. Int. J. Comput. Methods **12**, 1550002 (2015)
20. He, Z., Kotousov, A.: On evaluation of stress intensity factor from in-plane and transverse surface displacements. Exp. Mech. **56**, 1385–1393 (2016)
21. Koguchi, H., Yokoyama, K.: Stress analysis in three-dimensional joints with a crack at the vertex of the interface. Acta Mech. **228**, 2759–2773 (2017)
22. Soliman, E., Frederic, D., Moutou, P.R.: A new analytical generalization of the J and G-theta integrals for planar cracks in a three-dimensional medium. Theor. Appl. Fract. Mech. **94**, 101–109 (2018)
23. Chaudhuri, R.A.: On through-thickness distribution of stress intensity factors and energy release rates in the vicinity of crack fronts. Eng. Fract. Mech. **216**, 106478 (2019)
24. Ludwig, C., Rabold, F., Kuna, M., Schurig, M., Schlums, H.: Simulation of anisotropic crack growth behavior of nickel base alloys under thermomechanical fatigue. Eng. Fract. Mech. **224**, 106800 (2020)
25. Yi, D.K., Wang, T.C.: A new procedure for investigating three-dimensional stress fields in a thin plate with a through-thickness crack. Sci. China Phys. Mech. Astron. **61**, 064611 (2018)
26. Kishimoto, K., Aoki, S., Sakata, M.: On the path independent integral-J. Eng. Fract. Mech. **13**, 841–881 (1980)
27. Shih, C.F., Moran, B., Nakamura, T.: Energy release rate along a three-dimensional crack front in a thermally stressed body. Int. J. Fract. **30**(2), 79–102 (1986)

28. Chiarelli, M., Frediani, A.: A computation of the three-dimensional J-integral for elastic materials with a view to applications in fracture mechanics. Eng. Fract. Mech. **44**, 763–788 (1993)
29. Omer, N., Yosibash, Z.: On the path independency of the point-wise J integral in three-dimensions. Int. J. Fract. **136**, 1–36 (2005)
30. Hutchinson, J.W.: Singular behaviour at the end of a tensile crack in a hardening material. J. Mech. Phys. Solids **16**, 13–31 (1968)